

**^{99m}Tc-Duramycin SPECT imaging of early tumor response to targeted therapy: a
comparison with ¹⁸F-FDG PET**

Filipe Elvas*^{1,2}, Jan Boddart³, Christel Vangestel^{1,2}, Koon Pak⁴, Brian Gray⁴, Samir
Kumar-Singh³, Steven Staelens¹, Sigrid Stroobants^{1,2}, Leonie wyffels^{1,2}

¹Molecular Imaging Center Antwerp, University of Antwerp, Wilrijk, Belgium; ²Antwerp
University Hospital, Department of Nuclear Medicine, Edegem, Belgium; ³Laboratory of
Molecular Pathology, Cell Biology and Histology, University of Antwerp, Wilrijk, Belgium;
⁴Molecular Targeting Technologies, Inc., West Chester, PA, USA

For correspondence or reprints contact: Leonie wyffels, Department of Nuclear
Medicine, University Hospital Antwerp, Wilrijkstraat 10, 2650 Edegem, Belgium.

Email: leonie.wyffels@uza.be

Telephone number: +3238215699; Fax number: +3238253308

*PhD student, Email: filipe.elvas@uantwerpen.be

Department of Nuclear Medicine, University Hospital Antwerp, Wilrijkstraat 10, 2650
Edegem, Belgium.

Telephone number: +3238215692; Fax number: +3238253308

Financial support: GOA (G.0135.13)

Word count: 5000

Running title: ^{99m}Tc-Duramycin Imaging Therapy Response

ABSTRACT

Molecular imaging of cell death may provide a detailed readout of the cellular response to novel therapies and prognostic information on tumor treatment efficacy assisting in the design of individualized therapy. We compared the predictive power of cell death imaging using ^{99m}Tc -duramycin to current gold standard ^{18}F -FDG for treatment response evaluation after targeted therapy.

Methods: Early therapy response evaluation was assessed by ^{99m}Tc -duramycin SPECT and ^{18}F -FDG PET imaging in treatment-sensitive COLO205 and treatment-resistant HT29 human colorectal cancer xenografts 24 hours after a single dose of conatumumab or IgG1 control. The specificity of ^{99m}Tc -duramycin for apoptosis was assessed using ^{99m}Tc -linear duramycin control radiotracer. Radiotracer uptake was validated *ex vivo* by gamma-counting and autoradiography, and compared with caspase-3 activation (CC3) and DNA fragmentation (TUNEL). Data were analyzed with the Student's t test and Pearson correlation. All statistical tests were two-sided.

Results: COLO205 tumor uptake of ^{99m}Tc -duramycin was increased 7-fold from baseline in conatumumab- versus IgG1-treated control mice ($P<0.001$), in good correlation with histological analysis of apoptosis (CC3: $r=0.842$ and TUNEL: $r=0.894$, $P<0.001$). No response was detected in HT29 tumors. No change in ^{99m}Tc -linear duramycin uptake could be detected in COLO205 tumors after treatment, indicating specificity of the ^{99m}Tc -duramycin tumor signal. ^{18}F -FDG uptake was not significantly increased from baseline in conatumumab- versus IgG1-treated COLO205 and HT29 tumor bearing mice ($P=0.104$ and $P=0.779$, respectively), and did not correlate with immunohistochemical evidence of apoptosis.

Conclusion: We have demonstrated that ^{99m}Tc -duramycin specifically accumulates in apoptotic tumors where ^{18}F -FDG was not able to differentiate responding from non-responding tumors early after treatment. ^{99m}Tc -duramycin holds promise as a noninvasive imaging radiotracer for early treatment evaluation in the clinic.

Key Words: Cell death imaging; ^{99m}Tc -duramycin SPECT; response evaluation targeted therapy; colorectal cancer.

INTRODUCTION

Assessment of tumor response to anticancer therapy is of most importance to distinguish early responders from patients resistant to the treatment plan – enabling the so-called tailor-made therapeutic intervention. An early evaluation of therapeutic success of a given anticancer therapy could be of key importance to identify therapeutic failure and might prevent needless exposure of patients to treatment-associated side effects. Conventional anatomical imaging techniques, such as X-ray computed tomography (CT) and magnetic resonance imaging, are insufficient to early assess treatment responses (1). Molecular imaging techniques, such as positron emission tomography (PET) and single photon emission computed tomography (SPECT), offer a much more sensitive and specific tool for the noninvasive assessment of tumor physiology and metabolism, allowing an earlier assessment of therapy response and reducing treatment-related toxicity. ^{18}F -fluoro-2-deoxy-D-glucose (^{18}F -FDG) is the most commonly used PET tracer in routine clinical practice for monitoring response to therapy in oncology (reviewed in (2,3)). However, ^{18}F -FDG is not a cancer-specific probe, and significant uptake can occur in activated inflammatory cells (macrophages, neutrophils and fibroblasts) following therapy in both tumor and surrounding tissue (4).

The mechanisms of action of most anticancer drugs include the induction of cell death through multiple processes including apoptosis, necrosis as well as other modalities of cell death (5). For example, targeted therapy using conatumumab, a fully human monoclonal agonist antibody (IgG1) directed against the death receptor (DR) 5, has been shown to induce apoptosis in a number of *in vivo* models of human cancer, including colorectal cancer (6,7). An advantage of using targeted therapies is their

ability to selectively induce apoptosis in tumors and metastases (8), potentially reducing the treatment-related toxicity to the patient. Molecular imaging using cell death specific radiotracers offers a noninvasive, longitudinal, quantitative and sensitive approach to predict early responses in patients. In this context, clinically relevant imaging biomarkers of cell death have been identified (9-11). A well-studied one is aminophospholipid exposure (phosphatidylserine and phosphatidylethanolamine) in the cell membrane early in the course of apoptosis or during necrosis (12,13).

In the current study, we used ^{99m}Tc -duramycin, exploiting its high affinity and selectivity for phosphatidylethanolamine and optimal biodistribution profile (14,15), for *in vivo* SPECT imaging of cell death. Using small animal SPECT and PET imaging of treatment-resistant and treatment-sensitive models of human colorectal cancer, we aimed at directly comparing the performance of ^{99m}Tc -duramycin to the current clinical gold standard ^{18}F -FDG for early therapy response evaluation using targeted therapy.

MATERIALS AND METHODS

Animal Model

All the experimental procedures involving animals were approved by the local ethical committee (2015-14, University of Antwerp, Belgium). The xenograft models were generated by subcutaneous injection of COLO205 (2×10^6 in 100 μL DPBS, n=20) or HT29 (10×10^6 in 100 μL DPBS, n=17) tumor cells into the hind flank of 8-week-old female CD1-/- nude mice (body weight 20-25 g; Charles River Laboratories). When xenografts reached approximately 300 mm^3 , mice were treated with a single dose of conatumumab (1.5 mg/kg intraperitoneal, i.p.; Amgen, Inc.; n=18) or the corresponding

IgG1 isotype control (1.5 mg/kg i.p.; Amgen, Inc.; n=19). See Supplemental Methods for more information.

Radiotracer Preparation

Clinical-grade ^{18}F -FDG was prepared using a Fastlab cassette-based system (GE Healthcare). Radiosynthesis of $^{99\text{m}}\text{Tc}$ -duramycin and $^{99\text{m}}\text{Tc}$ -linear duramycin (Supplemental Fig.1) was performed as previously described (14). See Supplemental Methods for more information.

Imaging Studies

Treatment-induced changes in the tumors were assessed with $^{99\text{m}}\text{Tc}$ -duramycin SPECT and ^{18}F -FDG PET imaging. For longitudinal response assessment studies, $\mu\text{SPECT/CT}$ and $\mu\text{PET/CT}$ imaging was performed just before treatment (baseline) and 24 hours after therapy (Supplemental Fig. 2). Static whole-body SPECT imaging was performed 4 hours post radiotracer injection, as this imaging time point results in optimal tumor to background ratios as a result of the optimal blood clearance and rapid renal elimination that results in low background, as we previously demonstrated (14). Further details are in the Supplemental Methods.

***Ex Vivo* Validation**

After image acquisition mice were sacrificed by cervical dislocation. Tumor, blood and main organs were harvested immediately following sacrifice, weighed and the radioactivity in the samples was subsequently measured in an automated γ -counter

(Wizard² 2480, Perkin Elmer) using a ^{99m}Tc and ¹⁸F energy window of 121-159 keV and 450-650 keV, respectively. Data were expressed as percent injected dose per gram of tissue (%ID/g). Following γ -counting one half of the tumor was rapidly snap-frozen in tissue-Tek (OCT compound, VWR), sectioned (100 μ m) and exposed overnight to phosphor screen plates (Fujifilm, USA). Exposed plates were imaged in a Phosphor Imager system (FLA7000, GE Healthcare) for visualization of regional tracer distribution.

Immunohistochemistry

Adjacent tumor paraffin sections (5 μ m) were taken at regular intervals across the entire tumor volume, and used for histological analysis of apoptosis. Immunohistochemistry for cleaved caspase-3 (CC3) and TdT-mediated dUTP nick-end labeling (TUNEL) assay were performed. See Supplemental Methods for more information.

Statistical Analysis

Data were expressed as mean \pm standard error of the mean (SEM). Statistical analysis was performed using Prism v6.01 (GraphPad Software, USA). Statistical significance between two data sets was evaluated by the unpaired two-tailed Student's t test. Differences between groups were considered statistically significant if $P < 0.05$. For correlation analysis, Pearson's correlation coefficient was computed with $P < 0.05$ considered statistically significant.

RESULTS

Monitoring Drug-Induced Tumor Apoptosis

From the apoptosis-inducing effect of conatumumab established by others in colorectal cancer xenografts (6), 24 hours post single conatumumab or IgG1 treatment was selected as the optimal imaging time point for response assessment (Figs. 1 and 2). Uptake of ^{99m}Tc -duramycin in conatumumab-sensitive COLO205 tumors is shown in Figure 1A. The tracer uptake in these tumors was remarkably low at baseline (0.60 ± 0.05 %ID/mL and 0.64 ± 0.03 %ID/mL, for IgG1 and conatumumab-treated groups, respectively), and significantly increased by 7-fold 24 hours after conatumumab treatment (5.21 ± 0.76 %ID/mL; $P < 0.001$; Fig. 1A, left and right upper panels). IgG1 treatment did not result in an increased accumulation of ^{99m}Tc -duramycin in COLO205 xenografts (0.76 ± 0.07 %ID/mL; $P > 0.999$; Fig. 1A, right panels). In contrast, ^{18}F -FDG uptake in COLO205 tumors (Fig. 1B) was high at baseline (4.74 ± 0.75 %ID/mL and 4.88 ± 0.19 %ID/mL, for IgG1 and conatumumab groups, respectively) and did not significantly change at 24 hours post treatment (4.52 ± 0.12 %ID/mL and 5.76 ± 0.40 %ID/mL, $P = 0.777$ and $P = 0.082$, for IgG1 and conatumumab groups, respectively). Blood glucose was not different between IgG1 and conatumumab treatment groups nor changed significantly after treatment (Supplemental Table 1). Imaging with ^{99m}Tc -linear duramycin (Fig. 1C) showed a rapid tracer washout, as evidenced by the low absolute uptake values at baseline and 24 hours after treatment (IgG1: 0.07 ± 0.01 %ID/mL vs 0.07 ± 0.01 %ID/mL and conatumumab: 0.08 ± 0.01 %ID/mL vs 0.09 ± 0.01 %ID/mL, respectively), consistent with the compromised phosphatidylethanolamine binding of linear duramycin. Also, no significant increase from baseline was observed after either

IgG1 ($P > 0.999$) or conatumumab ($P > 0.999$) treatment in COLO205 tumors with ^{99m}Tc -linear duramycin. Changes in ^{99m}Tc -duramycin uptake after treatment were not accompanied by a reduction in tumor volume relative to pretreatment in COLO205 xenografts (Supplemental Fig. 3), indicating that ^{99m}Tc -duramycin uptake in treatment-responding tumors preceded changes in tumor volumes as assessed by caliper measurements.

To explore whether ^{99m}Tc -duramycin uptake in COLO205 tumors is specifically induced by the therapeutic apoptotic response to conatumumab, we additionally assessed radiotracer uptake in either IgG1- or conatumumab-treated human HT29 tumor xenografts; a tumor type well known for its weak expression of DR5 on the cell membrane (16) and resistance to conatumumab-induced cytotoxicity (6). In contrast to what was observed in COLO205 tumors, no significant difference in tumor-associated ^{99m}Tc -duramycin uptake between treatment groups was measured by μSPECT . Twenty-four hours treatment with either IgG1 (0.77 ± 0.11 %ID/mL; $P=0.081$) or conatumumab (0.90 ± 0.13 %ID/mL; $P=0.695$) showed no increase in uptake of ^{99m}Tc -duramycin in HT29 xenografts, with tracer uptake remaining at baseline levels in both groups (Fig. 2A). Similarly, for ^{18}F -FDG no significant change was observed in both IgG1 and conatumumab treatment groups, in comparison to baseline ($P > 0.999$), nor significant differences between both treatment groups ($P > 0.999$; Fig. 2B). The uptake of ^{99m}Tc -linear duramycin in conatumumab-treated HT29 tumor xenografts (Fig. 2C) remained at baseline levels, in agreement with data obtained for COLO205 tumors. In HT29 xenografts, both conatumumab and IgG1 antibody treatment did not result in a reduction in tumor volume after 24 hours relative to pretreatment (Supplemental Fig. 3).

Ex Vivo Validation

Tumor uptake and radiotracer biodistribution. To validate the obtained imaging results, tumor xenografts were harvested, the radioactivity was measured in a gamma-counter and the regional distribution of ^{99m}Tc -duramycin (Fig. 3) and ^{99m}Tc -linear duramycin (Supplemental Fig. 4) was assessed by autoradiography, immediately after imaging. As assessed by *ex vivo* γ -counting, the uptake of ^{99m}Tc -duramycin in COLO205 tumor tissue 24 hours after conatumumab treatment was 4.92 ± 0.66 %ID/g (Fig. 3A) and it was significantly higher than in the IgG1 group (0.60 ± 0.08 %ID/g; $P=0.003$). The uptake of ^{18}F -FDG in conatumumab-treated COLO205 tumors was high (2.71 ± 0.34 %ID/g) but not significantly different to the IgG1 control ($P=0.197$). The uptake of ^{99m}Tc -duramycin and ^{18}F -FDG in HT29 xenografts (1.43 ± 0.29 %ID/g and 2.10 ± 0.30 %ID/g, respectively; Fig. 3B) did not differ from the IgG1 control group ($P=0.526$ and $P=0.327$, respectively). Gamma-counting did not show any significant change in ^{99m}Tc -linear duramycin tumor uptake after conatumumab treatment when compared to IgG1 group for both COLO205 and HT29 tumors (Figs. 3A and B). After intravenous injection ^{99m}Tc -duramycin has favorable biodistribution, clearance and pharmacokinetic profiles. Previously we and others have shown that it quickly clears from circulation via the renal system, with low hepatic and gastrointestinal uptake (13-15). Radiotracer uptake in blood, muscle, liver, spleen and kidneys was not significantly changed by conatumumab treatment ($P > 0.999$), when compared to the IgG1 treated group (Table 1, Supplemental Tables 2 and 3 and Supplemental Fig. 5). The tumor-to-blood and tumor-to-muscle ratios of ^{99m}Tc -duramycin in COLO205 conatumumab-

treated xenografts were 14.93 ± 1.32 ($P=0.003$) and 30.80 ± 1.89 ($P<0.001$), respectively, and were significantly higher than those in the IgG1 group (Table 1). No statistically significant difference in the tumor-to-background ratios was found between conatumumab and IgG1-treated HT29 xenografts for all radiotracers. In spite of the known membrane disruptive effects of duramycin (17), the tracer concentrations of duramycin that are used for imaging did not result in any pharmacological or toxic effect (data not shown).

The higher uptake of ^{99m}Tc -duramycin in conatumumab-treated COLO205 tumors was further illustrated by the *ex vivo* autoradiography of tumor slices (Figs. 3C and D). Autoradiographs showed a regional accumulation of ^{99m}Tc -duramycin in the tumors and colocalization of increased radioactivity uptake within tumor areas where there was an elevated rate of apoptotic response, as demonstrated by increased levels of active caspase-3 immunoreactivity and TUNEL staining (Figs. 3C and D). In agreement with ^{99m}Tc -duramycin autoradiographs, CC3 immunoreactivity and TUNEL levels were modest in IgG1-treated COLO205 and in both conatumumab and IgG1-treated HT29 xenografts. In contrast, ^{99m}Tc -linear duramycin did not accumulate in the tumors with high apoptotic levels (Supplemental Fig. 4).

Relationship between radiotracer uptake and histology. To determine how well radiotracer uptake predicts response to therapy, quantification of caspase-3 activation and TUNEL staining was performed on whole tumor sections (Figs. 3C, D and 4; Supplemental Fig. 6). In agreement with ^{99m}Tc -duramycin uptake, 24 hours post-conatumumab treatment, COLO205 tumors were characterized by an elevation of

caspase-3 activation (9.6 ± 0.7 % vs 1.5 ± 0.5 % in IgG1 group; $P < 0.001$; Supplemental Fig. 6) and an increased number of DNA strand breaks (9.5 ± 1.9 % vs 0.9 ± 0.4 % in IgG1 group; $P < 0.001$; Supplemental Fig. 6), as assessed by TUNEL staining. These tumors also showed the presence of small clusters of cells, due to cell shrinkage, and dense nuclear chromatin fragments, characteristic of apoptotic cells, as seen by histological examination with hematoxylin and eosin stain (Supplemental Fig. 6). Figure 4 shows the scatterplots that demonstrate how well tumor response to therapy (cell death) can be predicted by radiotracer uptake (%ID/g) in the tumors. Animals injected with ^{99m}Tc -duramycin showed a good correlation (CC3: $r = 0.842$, $P < 0.001$ and TUNEL: $r = 0.894$, $P < 0.001$) between whole tumor mean radioactivity and cell death in histologic sections stained with CC3 and TUNEL (Figs. 4A and B), whereas no correlation was found either for ^{18}F -FDG (CC3: $r = 0.280$, $P = 0.333$ and TUNEL: $r = 0.132$, $P = 0.653$; Figs. 4C and D) nor for ^{99m}Tc -linear duramycin (CC3: $r = 0.170$, $P = 0.617$ and TUNEL: $r = 0.156$, $P = 0.628$; Supplemental Fig. 7).

DISCUSSION

In the clinic, the assessment of anticancer therapy response represents a major hurdle for therapy management of cancer patients. Resistance to chemotherapy and molecular-targeted therapy is often associated with dysregulation and suppression of cell death mechanisms in tumors (18). Since induction of cell death is a desired effect of most anticancer therapies, the early detection of the levels of cell death after therapy can be used as a surrogate endpoint for tumor response evaluation, and assist in the design of appropriate individualized and optimized therapies. Noninvasive molecular

imaging strategies to detect apoptosis represent an attractive alternative to histological assessment of apoptosis routinely performed in the clinic through invasive tumor biopsies. The latter may fail to predict therapeutic response due to underlying genetic and phenotypic heterogeneity of tumors (19). Here, we compared the performance of a novel apoptosis imaging agent, ^{99m}Tc -duramycin, to the most widely used PET radiotracer in clinic, ^{18}F -FDG, in treatment-resistant (HT29) and treatment-sensitive (COLO205) human colorectal cancer xenografts for assessment of response to targeted therapy using conatumumab. This anti-DR5 monoclonal antibody is capable of inducing apoptosis in human colon, lung, and pancreas cancer cell lines (6). The known expression of DR5 in tumors of the colorectum (16) was accurately reflected by extensive apoptotic cell death and elevated caspase-3 activity induced by conatumumab in COLO205 xenografts as observed here and elsewhere (6,7,20).

Because in patients only a small increase in the levels of tumor apoptosis (2 to 6-fold) is to be expected after anticancer therapy (10), cell death-targeting radiotracers should be sensitive enough to allow imaging of therapy-induced apoptosis. Among the different tracers, radiolabeled annexin V, which binds to phosphatidylserine, has been widely used to image drug-induced cell death. Labeling with both SPECT (^{99m}Tc) and PET (^{18}F , ^{68}Ga) radioisotopes and successful imaging of treatment-induced cell death in human lymphoma, lung and breast cancer (21) have been reported. Previously our group has demonstrated the potential of ^{99m}Tc -duramycin to visualize radiotherapy- (15) and chemotherapy-induced (14,15) apoptosis. The sensitivity for apoptosis imaging was demonstrated by a 3-fold increase in ^{99m}Tc -duramycin uptake (2 %ID/g) in colorectal cancer xenografts treated with irinotecan in combination with oxaliplatin versus vehicle

treated tumors, in good correlation with the tumor apoptotic response (4 to 7-fold increase). In the current study, the high apoptotic response induced by conatumumab was followed by a remarkable 7-fold increase in ^{99m}Tc -duramycin accumulation (5 %ID/g) in COLO205 tumors, in very good correlation with histological evidence of apoptosis in tumors. Conatumumab-resistant HT29 tumors showed low levels of ^{99m}Tc -duramycin uptake after treatment which corresponded to a lack of cell death induction, thus showing the high sensitivity of ^{99m}Tc -duramycin for predicting early response to therapy. Less encouraging results have been obtained when using the small molecule caspase-3 targeting tracer ^{18}F -ICMT-11, which has previously shown potential to image apoptosis and is currently in clinical trials (22). ^{18}F -ICMT-11 was unable to detect a 5-fold increase in apoptosis induced by carboplatin treatment in human non-small cell lung carcinoma xenografts (23), and only a disappointingly low ^{18}F -ICMT-11 uptake (0.5-fold increase from baseline) was found in highly apoptotic tumors, with low tumor to background ratios (24), following etoposide/cyclophosphamide combination treatment of lymphoma tumor bearing mice. Additionally, in clear contrast to ^{99m}Tc -duramycin, ^{18}F -ICMT-11 showed a suboptimal pharmacokinetic profile, with high retention of radioactivity in the liver and intestines (25), which may limit its value for imaging the abdominal region. Given the limitations of the existing radiotracers, a novel strategy using a caspase-3 sensitive nanoaggregation PET tracer, ^{18}F -C-SNAT, was developed to overcome the low tumor accumulation *in vivo* (26). Despite early promise, a recent study demonstrated that while high levels of tumor apoptosis were present after etoposide treatment in lymphoma tumor bearing mice, only moderate accumulation of ^{18}F -C-SNAT (<3 %ID/g) was found in the tumors (27). Another potential advantage of

^{99m}Tc -duramycin over its caspase-3 targeting counterparts is the fact that it can detect therapy-induced necrosis. Because anticancer therapy may have an apoptosis- and necrosis-inducing effect in tumors (28), ^{99m}Tc -duramycin can theoretically bind both apoptotic and necrotic tumor cells, potentially leading to an enhanced SPECT signal in responding tumors. The presence of necrosis in some tumors, evidenced here by hematoxylin and eosin staining, may have contributed to the higher baseline uptake of ^{99m}Tc -duramycin in HT29 versus COLO205 tumors.

Specificity of ^{99m}Tc -duramycin for detecting phosphatidylethanolamine in apoptotic cells was demonstrated by using a ^{99m}Tc labeled linearized duramycin molecule (^{99m}Tc -linear duramycin) that lacks affinity for phosphatidylethanolamine. This control peptide is an inactive form of duramycin that does not bind to phosphatidylethanolamine and has a minimally altered structure and the molecular weight of duramycin, as previously described by others (29,30). ^{99m}Tc -linear duramycin exhibited a rapid blood clearance and the biodistribution was prominent in the kidneys and liver similarly to ^{99m}Tc -duramycin. Upon conatumumab treatment the uptake of ^{99m}Tc -linear duramycin in both colorectal cancer xenografts stayed at baseline with no correlation with the levels of apoptosis in the tumors. ^{99m}Tc -linear duramycin showed little nonspecific uptake and supports specific phosphatidylethanolamine targeting of ^{99m}Tc -duramycin in the tumors.

Furthermore, in HT29 xenografts, ^{99m}Tc -duramycin uptake remained at baseline levels after drug treatment. Immunohistochemical and histological analysis of the tumors was in agreement with these findings, showing little or no evidence of drug activity. Thus, ^{99m}Tc -duramycin SPECT imaging reflected the lack of drug efficacy in this

tumor, demonstrating that it can differentiate responders from non-responders already early in the course of therapy, aiding clinicians in their decision to stop or prolong the therapy regimen.

^{18}F -FDG PET is an important clinical standard used for evaluation of cancer treatment response in lymphoma (31), and in breast (32), lung (33) and colorectal carcinoma (34). The uptake of this radiopharmaceutical is tied to the glycolytic metabolic rate of viable tumor cells (Warburg effect). Therefore, changes in ^{18}F -FDG uptake do not provide direct information on cell death, but only act as an indirect measure of tumor response. Importantly, response to treatment as evidenced by increased $^{99\text{m}}\text{Tc}$ -duramycin tumor uptake was seen as early as 24 hours after therapy, while only a small but non-statistically significant increase could be observed in ^{18}F -FDG uptake in treatment sensitive tumors. Since apoptosis is an energy-dependent process, and drug treatment increased apoptosis in these tumors it may be hypothesized that this limited positive response on ^{18}F -FDG PET was the result of a subsequent increase in glucose (or ^{18}F -FDG) uptake by the therapy responding tumors – the so-called metabolic flare phenomenon (35). Moreover, it is well known that activated granulocytes and mononuclear cells use glucose as an energy source (36,37). It is therefore not surprising that ^{18}F -FDG accumulates in a variety of inflammatory processes, which are often present following drug or radiation therapy (38) and can give rise to false-positive results. In summary, we show here that $^{99\text{m}}\text{Tc}$ -duramycin allows specific longitudinal imaging of drug-induced apoptosis in tumors with high sensitivity. In comparison, ^{18}F -FDG was not able to distinguish responding from non-responding tumors, thus

performing poorly in assessing tumor response in the first 24 hours after initiation of conatumumab therapy.

CONCLUSION

These findings indicate the potential usefulness of ^{99m}Tc -duramycin SPECT imaging for early therapy response assessment after targeted therapy. Along with our previous reports showing fast blood and renal clearance, low accumulation in non-targeted organs, favorable dosimetry, and metabolic stability, this study further supports clinical translation of ^{99m}Tc -duramycin for therapy response in cancer patients.

DISCLOSURE

Brian Gray and Koon Pak are employees of Molecular Targeting Technologies, Inc.

ACKNOWLEDGMENTS

The authors gratefully acknowledge Philippe Joye, Caroline Berghmans and Steven Deleye for their assistance with small animal imaging. Conatumumab (AMG 655) and IgG1 isotype control antibodies were kindly supplied by Amgen, Inc.

REFERENCES

1. Wahl RL, Jacene H, Kasamon Y, Lodge MA. From RECIST to PERCIST: Evolving Considerations for PET response criteria in solid tumors. *J Nucl Med.* 2009;50 Suppl 1:122S-150S.
2. Kostakoglu L, Goldsmith SJ. 18F-FDG PET evaluation of the response to therapy for lymphoma and for breast, lung, and colorectal carcinoma. *J Nucl Med.* 2003;44:224-239.
3. Ben-Haim S, Ell P. 18F-FDG PET and PET/CT in the evaluation of cancer treatment response. *J Nucl Med.* 2009;50:88-99.
4. Chang JM, Lee HJ, Goo JM, et al. False positive and false negative FDG-PET scans in various thoracic diseases. *Korean J Radiol.* 2006;7:57-69.
5. Rello-Varona S, Herrero-Martin D, Lopez-Aleman R, Munoz-Pinedo C, Tirado OM. "(Not) all (dead) things share the same breath": identification of cell death mechanisms in anticancer therapy. *Cancer Res.* 2015;75:913-917.
6. Kaplan-Lefko PJ, Graves JD, Zoog SJ, et al. Conatumumab, a fully human agonist antibody to death receptor 5, induces apoptosis via caspase activation in multiple tumor types. *Cancer Biol Ther.* 2010;9:618-631.
7. Zoog SJ, Ma CY, Kaplan-Lefko PJ, et al. Measurement of conatumumab-induced apoptotic activity in tumors by fine needle aspirate sampling. *Cytometry A.* 2010;77:849-860.
8. Johnstone RW, Frew AJ, Smyth MJ. The TRAIL apoptotic pathway in cancer onset, progression and therapy. *Nat Rev Cancer.* 2008;8:782-798.
9. Neves AA, Brindle KM. Imaging cell death. *J Nucl Med.* 2014;55:1-4.
10. De Saint-Hubert M, Bauwens M, Mottaghy FM. Molecular imaging of apoptosis for early prediction of therapy efficiency. *Curr Pharm Des.* 2014;20:2319-2328.
11. De Saint-Hubert M, Prinsen K, Mortelmans L, Verbruggen A, Mottaghy FM. Molecular imaging of cell death. *Methods.* 2009;48:178-187.
12. Blankenberg FG, Katsikis PD, Tait JF, et al. Imaging of apoptosis (programmed cell death) with 99mTc annexin V. *J Nucl Med.* 1999;40:184-191.

13. Zhao M, Li Z, Bugenhagen S. 99mTc-labeled duramycin as a novel phosphatidylethanolamine-binding molecular probe. *J Nucl Med.* 2008;49:1345-1352.
14. Elvas F, Vangestel C, Ropic S, et al. Characterization of [(99m)Tc]Duramycin as a SPECT Imaging Agent for Early Assessment of Tumor Apoptosis. *Mol Imaging Biol.* 2015;17:838-847.
15. Elvas F, Vangestel C, Pak K, et al. Early Prediction of Tumor Response to Treatment: Preclinical Validation of 99mTc-Duramycin. *J Nucl Med.* 2016;57:805-811.
16. Oliver PG, LoBuglio AF, Zinn KR, et al. Treatment of human colon cancer xenografts with TRA-8 anti-death receptor 5 antibody alone or in combination with CPT-11. *Clin Cancer Res.* 2008;14:2180-2189.
17. Rzeznicka, II, Sovago M, Backus EH, et al. Duramycin-induced destabilization of a phosphatidylethanolamine monolayer at the air-water interface observed by vibrational sum-frequency generation spectroscopy. *Langmuir.* 2010;26:16055-16062.
18. Wong RS. Apoptosis in cancer: from pathogenesis to treatment. *J Exp Clin Cancer Res.* 2011;30:87.
19. Bedard PL, Hansen AR, Ratain MJ, Siu LL. Tumour heterogeneity in the clinic. *Nature.* 2013;501:355-364.
20. Rosevear HM, Lightfoot AJ, Griffith TS. Conatumumab, a fully human mAb against death receptor 5 for the treatment of cancer. *Curr Opin Investig Drugs.* 2010;11:688-698.
21. Belhocine T, Steinmetz N, Hustinx R, et al. Increased uptake of the apoptosis-imaging agent (99m)Tc recombinant human annexin V in human tumors after one course of chemotherapy as a predictor of tumor response and patient prognosis. *Clin Cancer Res.* 2002;8:2766-2774.
22. Challapalli A, Kenny LM, Hallett WA, et al. 18F-ICMT-11, a caspase-3-specific PET tracer for apoptosis: biodistribution and radiation dosimetry. *J Nucl Med.* 2013;54:1551-1556.
23. Witney TH, Fortt R, Aboagye EO. Preclinical assessment of carboplatin treatment efficacy in lung cancer by 18F-ICMT-11-positron emission tomography. *PLoS One.* 2014;9:e91694.
24. Glaser M, Goggi J, Smith G, et al. Improved radiosynthesis of the apoptosis marker 18F-ICMT11 including biological evaluation. *Bioorg Med Chem Lett.* 2011;21:6945-6949.

25. Nguyen QD, Lavdas I, Gubbins J, et al. Temporal and spatial evolution of therapy-induced tumor apoptosis detected by caspase-3-selective molecular imaging. *Clin Cancer Res.* 2013;19:3914-3924.
26. Shen B, Jeon J, Palner M, et al. Positron emission tomography imaging of drug-induced tumor apoptosis with a caspase-triggered nanoaggregation probe. *Angew Chem Int Ed Engl.* 2013;52:10511-10514.
27. Witney TH, Hoehne A, Reeves RE, et al. A systematic comparison of 18F-C-SNAT to established radiotracer imaging agents for the detection of tumor response to treatment. *Clin Cancer Res.* 2015;21:3896-3905.
28. Galluzzi L, Vitale I, Vacchelli E, Kroemer G. Cell death signaling and anticancer therapy. *Front Oncol.* 2011;1:1-18.
29. Stafford JH, Thorpe PE. Increased exposure of phosphatidylethanolamine on the surface of tumor vascular endothelium. *Neoplasia.* 2011;13:299-308.
30. Liu Z, Larsen BT, Lerman LO, et al. Detection of atherosclerotic plaques in ApoE-deficient mice using (99m)Tc-duramycin. *Nucl Med Biol.* 2016;43:496-505.
31. Cheson BD, Fisher RI, Barrington SF, et al. Recommendations for initial evaluation, staging, and response assessment of Hodgkin and non-Hodgkin lymphoma: the Lugano classification. *J Clin Oncol.* 2014;32:3059-3068.
32. Groheux D, Majdoub M, Sanna A, et al. Early Metabolic Response to Neoadjuvant Treatment: FDG PET/CT Criteria according to Breast Cancer Subtype. *Radiology.* 2015;277:358-371.
33. Marcus C, Paidpally V, Antoniou A, Zaheer A, Wahl RL, Subramaniam RM. 18F-FDG PET/CT and lung cancer: value of fourth and subsequent posttherapy follow-up scans for patient management. *J Nucl Med.* 2015;56:204-208.
34. Delbeke D, Martin WH. FDG PET and PET/CT for colorectal cancer. *Methods Mol Biol.* 2011;727:77-103.
35. Findlay M, Young H, Cunningham D, et al. Noninvasive monitoring of tumor metabolism using fluorodeoxyglucose and positron emission tomography in colorectal cancer liver metastases: correlation with tumor response to fluorouracil. *J Clin Oncol.* 1996;14:700-708.
36. Weisdorf DJ, Craddock PR, Jacob HS. Glycogenolysis versus glucose transport in human granulocytes: differential activation in phagocytosis and chemotaxis. *Blood.* 1982;60:888-893.

- 37.** Lander HM, Sehajpal P, Levine DM, Novogrodsky A. Activation of human peripheral blood mononuclear cells by nitric oxide-generating compounds. *J Immunol.* 1993;150:1509-1516.
- 38.** Kubota R, Yamada S, Kubota K, Ishiwata K, Tamahashi N, Ido T. Intratumoral distribution of fluorine-18-fluorodeoxyglucose in vivo: high accumulation in macrophages and granulation tissues studied by microautoradiography. *J Nucl Med.* 1992;33:1972-1980.

Figures

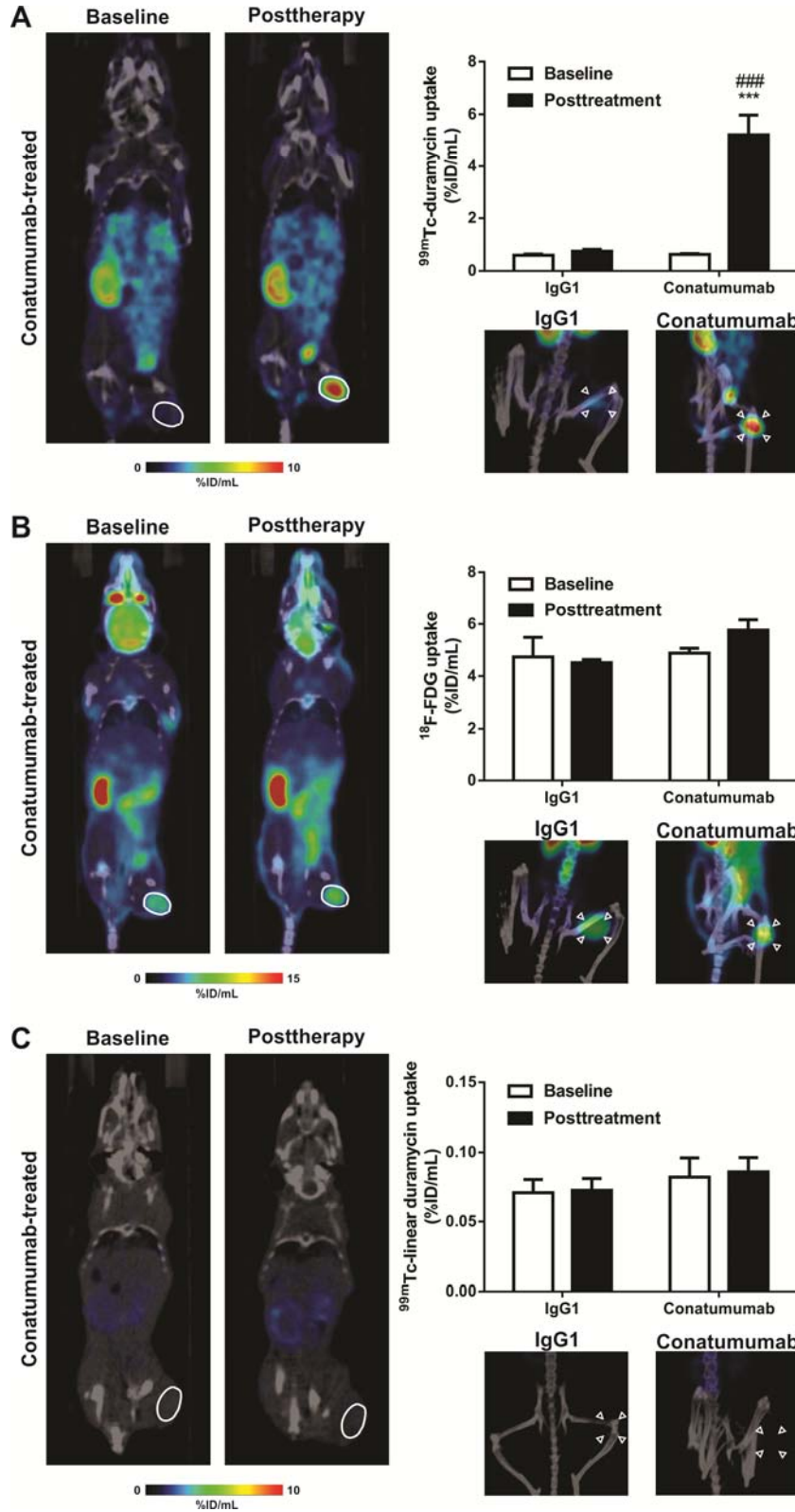


FIGURE 1. *In vivo* evaluation of ^{99m}Tc -duramycin (A), ^{18}F -FDG (B) and ^{99m}Tc -linear duramycin (C) uptake in IgG1- or conatumumab-treated COLO205 xenografts. Left panel: representative coronal $\mu\text{SPECT}/\text{CT}$ or $\mu\text{PET}/\text{CT}$ images of a COLO205 tumor-bearing animal at baseline and 24 hours after conatumumab treatment. Tumors are encircled. Right upper panel: quantification of radiotracer uptake in COLO205 tumor xenografts (***, $P < 0.001$, significantly different from baseline; ###, $P < 0.001$, significantly different from IgG1 post treatment). Right lower panel: maximum intensity projections showing radiotracer accumulation in COLO205 tumors 24 hours after IgG1 or conatumumab treatment. Arrow heads point to COLO205 tumors.

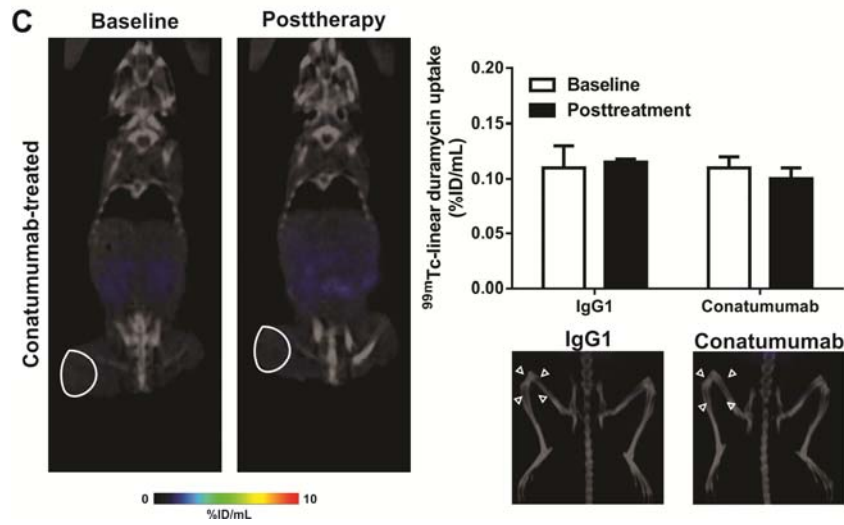
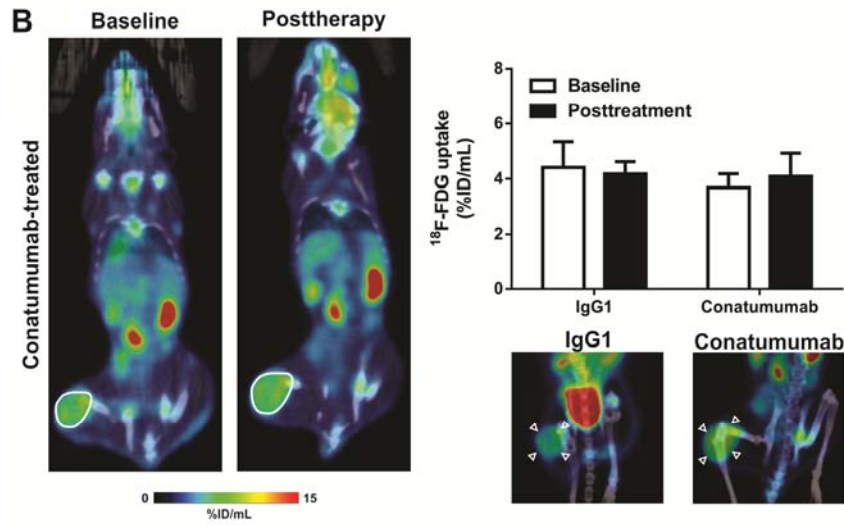
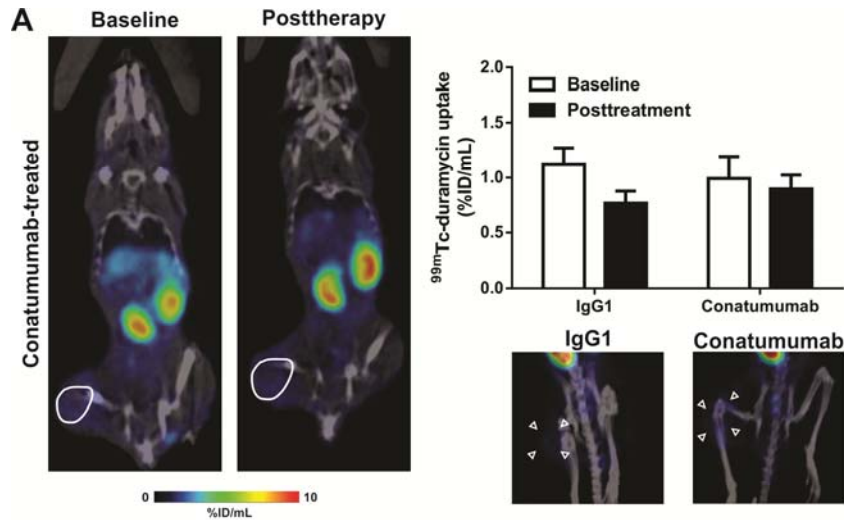


FIGURE 2. *In vivo* evaluation of ^{99m}Tc -duramycin (A), ^{18}F -FDG (B) and ^{99m}Tc -linear duramycin (C) uptake in IgG1- or conatumumab-treated HT29 xenografts. Left panel: representative coronal $\mu\text{SPECT/CT}$ or PET/CT images of a HT29 tumor-bearing animal at baseline and 24 hours after conatumumab treatment. Tumors are encircled. Right upper panel: quantification of radiotracer uptake in HT29 tumor xenografts. Right lower panel: maximum intensity projections showing radiotracer accumulation in HT29 tumors 24 hours after IgG1 or conatumumab treatment. Arrow heads point to HT29 tumors.

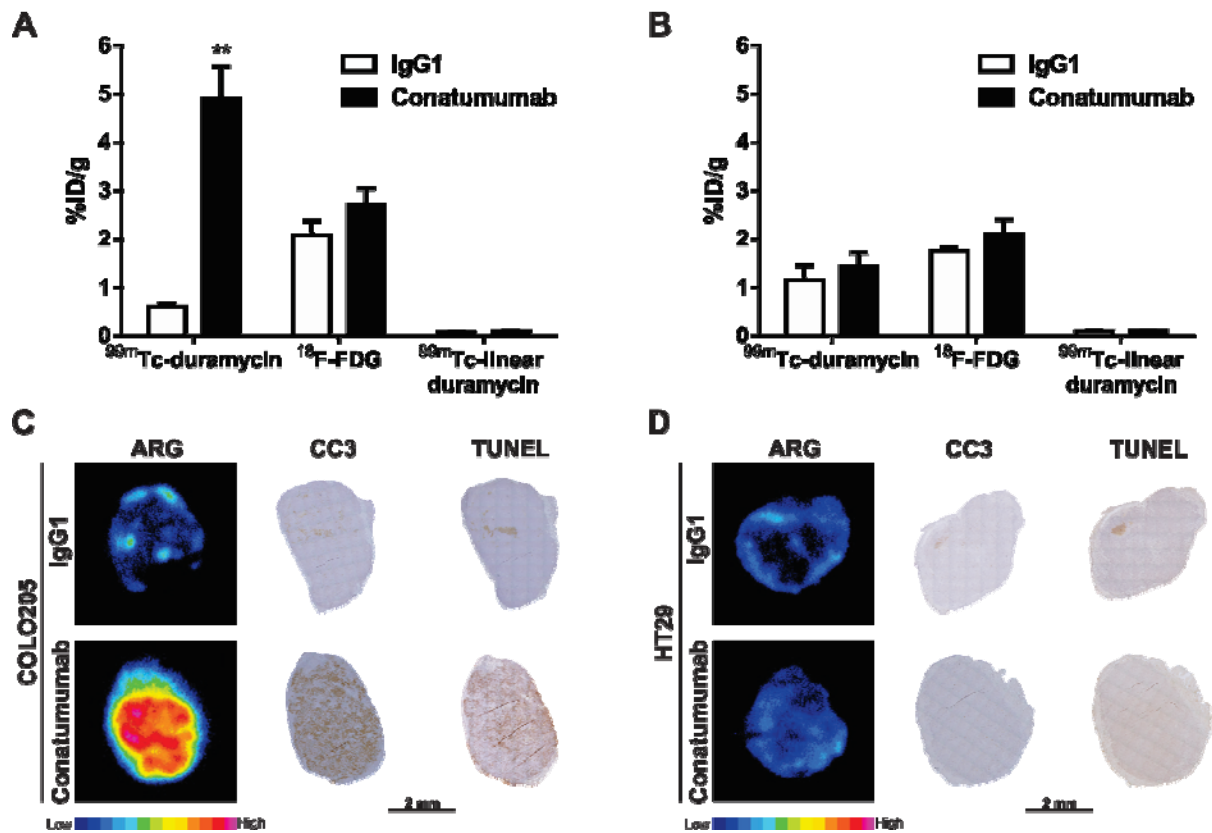


FIGURE 3. *Ex vivo* evaluation of radiotracer uptake and tumor apoptosis. Quantification of radiotracer uptake by gamma-counting of excised COLO205 (A) and HT29 (B) tumors. **, $P=0.003$, significantly different from IgG1. Representative pseudo-color autoradiography (ARG) and microscopy images of adjacent COLO205 (C) and HT29 (D) whole tumor slices stained for cleaved caspase-3 (CC3) and TUNEL from mice injected with ^{99m}Tc-duramycin.

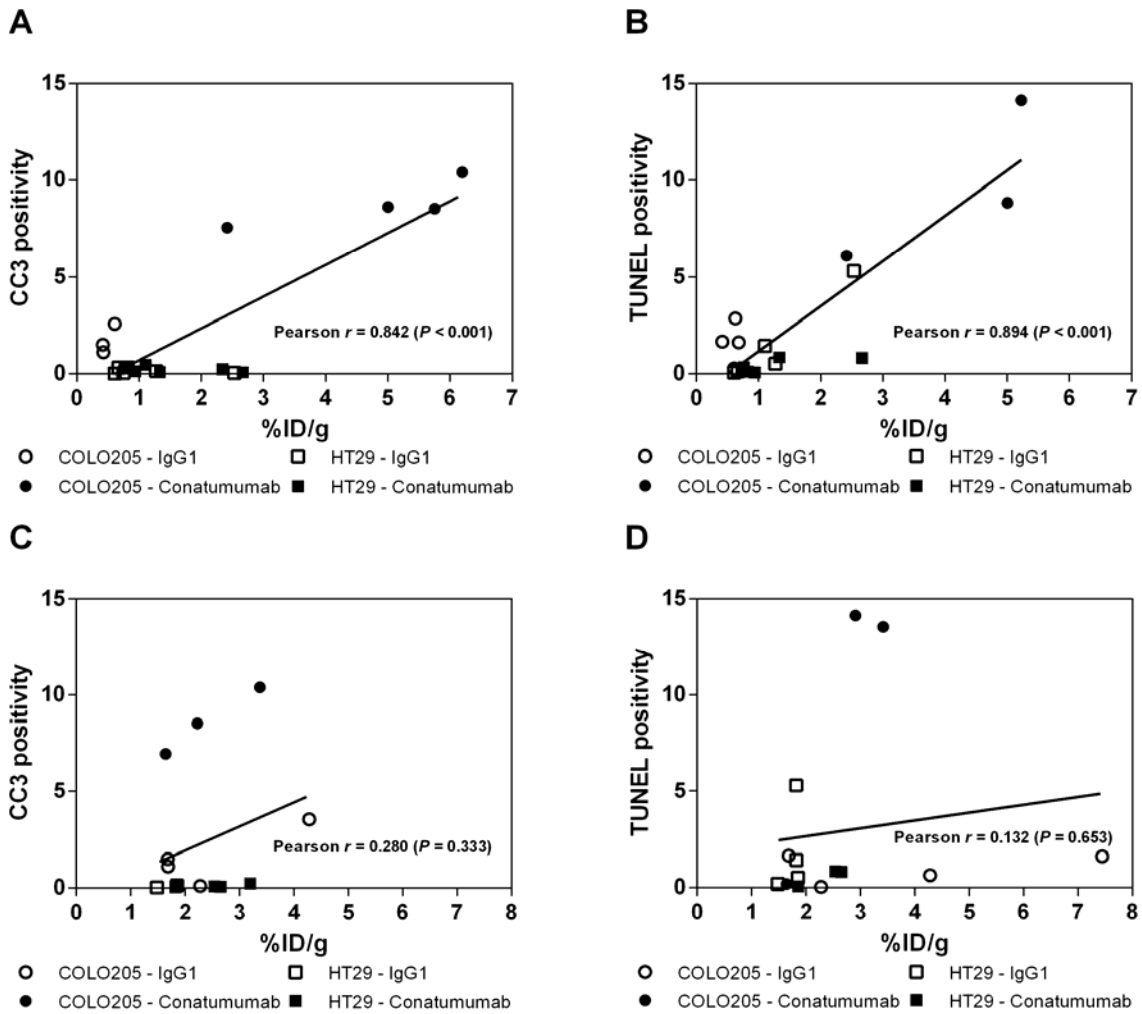


FIGURE 4. Correlation analysis of radiotracer uptake to histological measurement of tumor cell death. CC3 and TUNEL staining (cell death) were compared with tumor-associated ^{99m}Tc -duramycin (A and B, respectively) and ^{18}F -FDG (C and D, respectively) radioactivity measured *ex vivo* in the tumors (%ID/g).

Tables

TABLE 1. Uptake of ^{99m}Tc-duramycin in COLO205 and HT29 xenografts 24 hours post treatment and tumor-to-background ratios

Parameter	COLO205		HT29	
	IgG1	Conatumumab	IgG1	Conatumumab
Blood uptake (%ID/g)	0.39 ± 0.08	0.39 ± 0.08	0.34 ± 0.01	0.36 ± 0.01
Muscle uptake (%ID/g)	0.15 ± 0.02	0.16 ± 0.02	0.15 ± 0.01	0.15 ± 0.01
T/B ratio	1.83 ± 0.32	14.93 ± 1.32**	3.41 ± 0.84	3.96 ± 0.78
T/M ratio	4.45 ± 0.92	30.80 ± 1.89***	7.40 ± 1.66	9.53 ± 1.85

** , $P=0.003$; *** , $P<0.001$. Data are mean ± SEM

SUPPLEMENTAL METHODS

Animal Model

COLO205 (ATCC-CCL-222) and HT29 (ATCC-HTB-38) human colorectal adenocarcinoma cells were grown in complete RPMI1640 and DMEM medium, respectively, supplemented with 2 mM L-glutamine, 1 mM sodium pyruvate, 10% fetal bovine serum and 100 U/mL penicillin plus 100 mg/mL streptomycin (Life Technologies). Both cell lines were cultured at 37°C in a humidified atmosphere containing 5% CO₂. After subcutaneous cell injection, tumor dimensions were measured daily using a digital caliper, with tumor volumes calculated according to the formula: (length x width²)/2. Blood glucose levels were measured (in duplicate) before ¹⁸F-FDG PET scans from a drop of blood from the tail vein using a blood glucose meter (One Touch Ultra 2, Lifescan). Mice were subjected to μ SPECT/CT followed by μ PET/CT imaging just before (baseline) and 24 hours after therapy for treatment-response assessment as depicted in Supplemental Figure 2.

Control Peptide Preparation

To confirm the binding specificity of ^{99m}Tc-duramycin, a 19-amino acid linear control peptide (American Peptide Corporation) in which the thioether-linked amino acids are replaced by alanines and arginines are substituted for lysines (Ala-Arg-Gln-Ala-Ala-Ala-Phe-Gly-Pro-Phe-Ala-Phe-Val-Ala-Asp-Gly-Asn-Ala-Arg) was obtained. The linear peptide was reacted with HYNIC-NHS ester in DMSO purified by HPLC and radiolabeled with ^{99m}Tc (^{99m}Tc-linear duramycin; Supplemental Fig. 1A) as previously described for ^{99m}Tc-duramycin (18). The mass spectrum of HYNIC-linear duramycin

control peptide showed the desired peptide mass. MS (ESI+) Calcd. [M+H]⁺: 2112; found: 2112 (Supplemental Fig. 1B).

Imaging Studies

All mice were fasted overnight (10 hours), after which they received an intravenous (i.v.) injection of ~37 MBq ^{99m}Tc-duramycin or ^{99m}Tc-linear duramycin via the lateral tail vein at baseline and, 24 hours after treatment. Static whole-body SPECT imaging was performed using a μ SPECT/CT scanner (VECTor/CT, MILabs) equipped with 75 pinholes of 1 mm, followed by CT acquisition (45 kV and 615 μ A) for attenuation correction and anatomical coregistration with SPECT images, as described before (1). Mice were anesthetized through isoflurane inhalation (5% for induction and 2% for maintenance) and kept at constant body temperature during the scans. SPECT images were reconstructed with ordered-subsets expectation maximization (10 iterations, 16 subsets) and 1.2 mm³ voxel size, and smoothed with a three dimensional isotropic Gaussian filter of 1 mm for visualization purposes. A 20% energy window centered at 140 keV photopeak was used. Immediately after μ SPECT/CT imaging, while still anesthetized, the mice received an injection of 18.5 MBq ¹⁸F-FDG, via a tail vein catheter, followed by a 30 minutes uptake period. After this, CT imaging was performed (80 keV, 500 μ A, 220° rotation with 120 rotation steps) for PET data attenuation correction and anatomical reference (Siemens Inveon μ PET/CT scanner). Static whole-body ¹⁸F-FDG μ PET images were next acquired over 20 minutes. The CT acquisitions were analytically reconstructed using the Feldkamp algorithm to a 352 x 352 x 606 matrix with 0.223 mm voxels. The μ PET data were reconstructed using 2 iterations with 16 subsets of the three-dimensional ordered-subset expectation maximization

(OSEM3D) and 18 maximum a posteriori (MAP) iterations, including scatter and attenuation correction, resulting in a 128 x 128 x 159 matrix of 0.77 x 0.77 x 0.79 mm voxels (2).

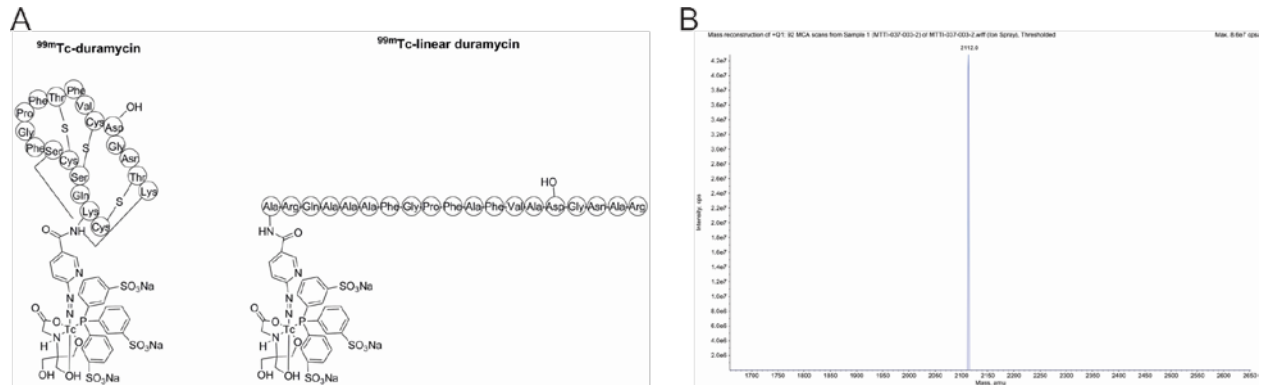
Based on the size of the scanner's field of view (FOV), volumes of interest (VOIs) for the subcutaneous tumors were outlined on the CT images using PMOD v3.3 (PMOD Technologies). Radiotracer uptake was obtained from mean voxel intensity values within the delineated VOIs and then converted to Megabecquerels per milliliter (MBq/mL) using the calibration factor determined for the VECTor/CT μ SPECT and Inveon μ PET systems. The image VOI-derived percent injected dose per mL (%ID/mL) was calculated as [total radioactivity concentration in the VOI at the time of scan (kBq/mL)/total radioactivity injected (kBq) x 100].

Immunohistochemistry

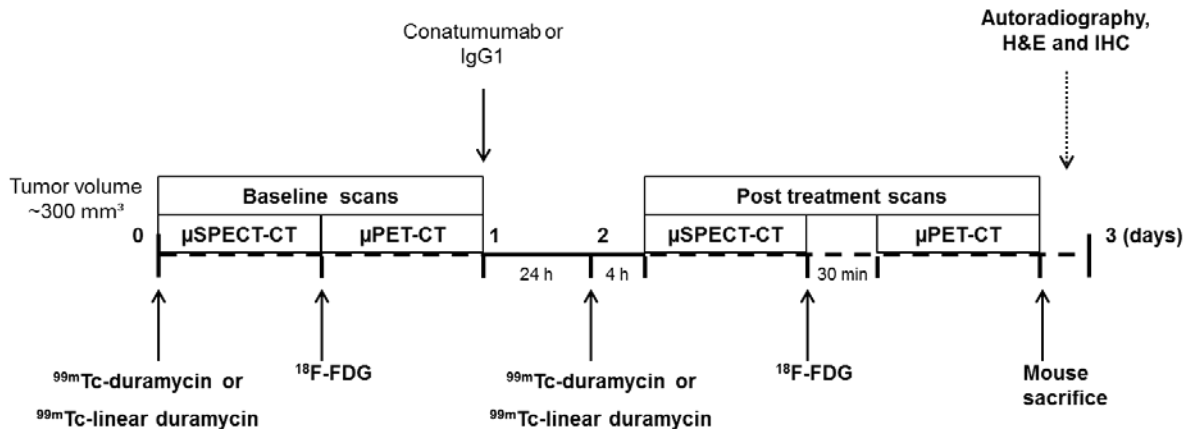
Tumors were fixed for 48 hours in 10% buffered formalin, and transferred to 70% ethanol until paraffin embedding. Immunohistochemistry for cleaved caspase-3 (CC3, rabbit monoclonal anti-CC3, 1:400 dilution, Cell Signaling Technology) and TdT-mediated dUTP nick-end labeling (TUNEL) assay (Promega) were carried out according to the manufacturer's instructions. The sections were counterstained with Ehrlich's hematoxylin. Tumors were also stained using standard hematoxylin and eosin (H&E) protocol and evaluated by a pathologist (S. Kumar-Singh). Light microscopic images were grabbed using a AxioScope A1 microscope (Zeiss) coupled with a Olympus UC30 color camera. Quantification of apoptosis was performed by calculating the percentage of CC3- and TUNEL-stained area across three non-sequential whole-tumor sections

using IHC profiler plug-in for ImageJ v1.47, as previously described (3). Seven to nine tumors were evaluated per treatment (conatumumab- or IgG1-treated) and tumor type (COLO205 or HT29). Mean percentage of positive stained area per tumor was used to calculate differences between groups. Apoptosis levels were correlated to the corresponding *ex vivo* radiotracer uptake in the tumor.

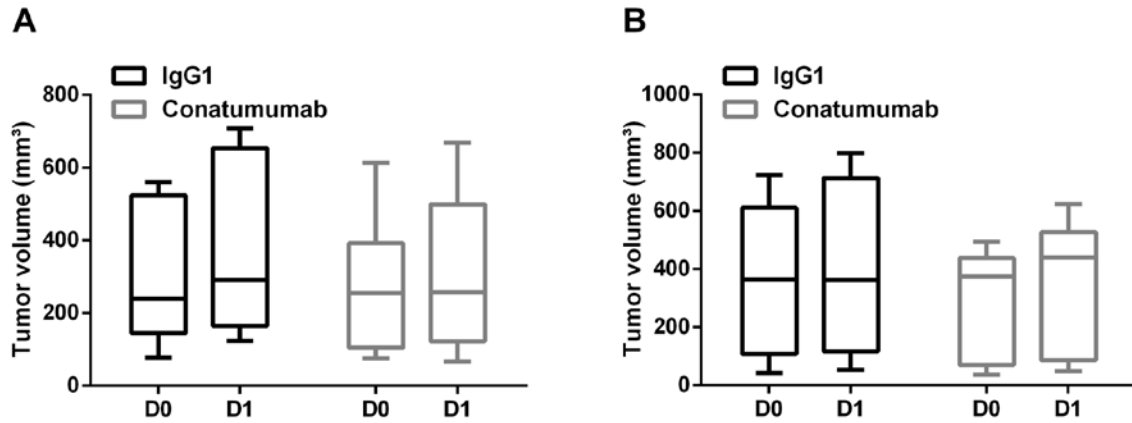
SUPPLEMENTAL FIGURES



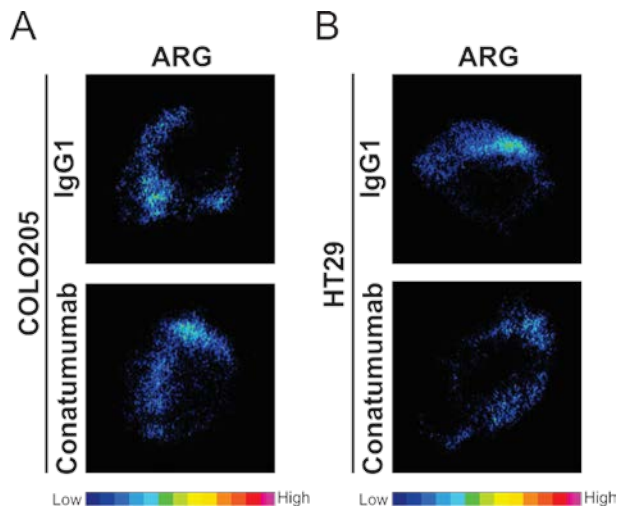
Supplemental Figure 1. Chemical structure for ^{99m}Tc -duramycin and ^{99m}Tc -linear duramycin (A). Mass spectrum of HYNIC-linear duramycin control peptide (B) showing the desired peptide mass. MS (ESI+) Calcd. $[\text{M}+\text{H}]^+$: 2112; found: 2112.



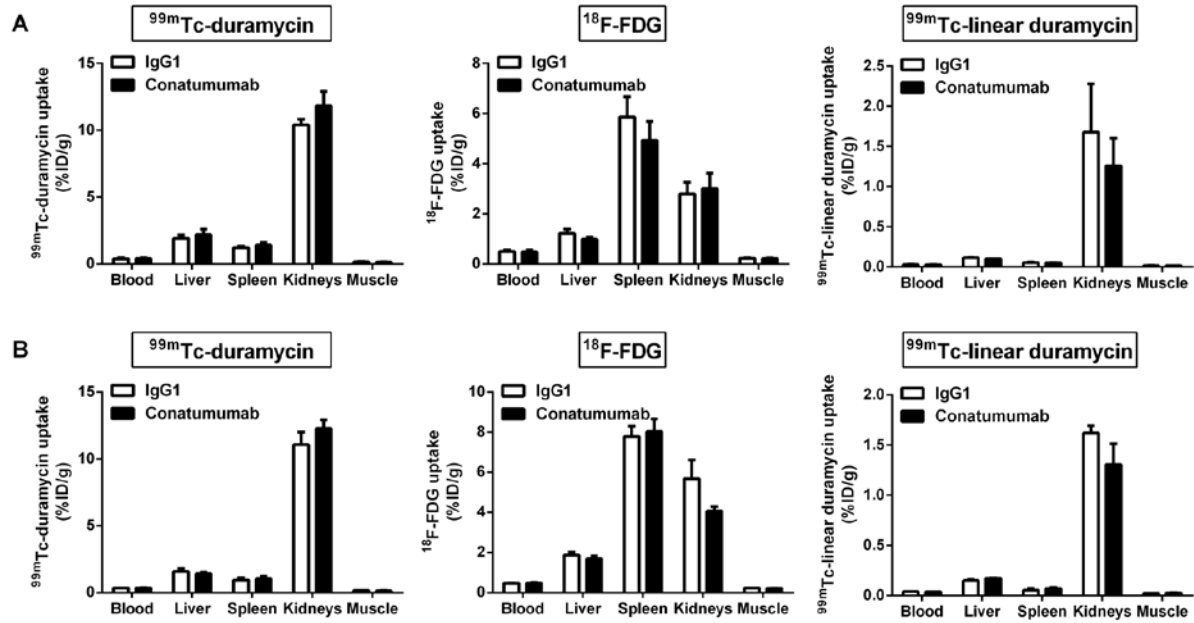
Supplemental Figure 2. Schematic representation of the experimental protocol using ^{99m}Tc -duramycin or ^{99m}Tc -linear duramycin SPECT/CT and ^{18}F -FDG PET/CT imaging in tumor-bearing mice treated with conatumumab or IgG1 control. H&E = hematoxylin and eosin; IHC = immunohistochemistry.



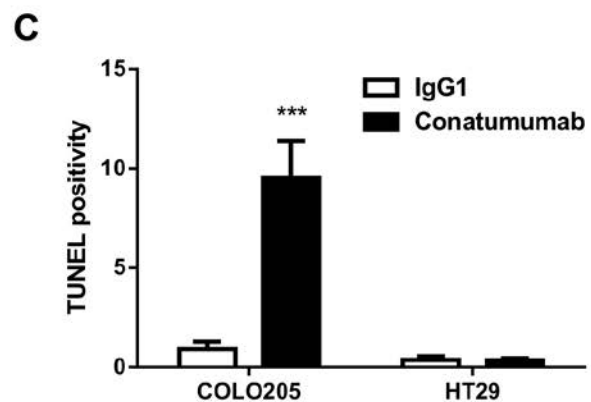
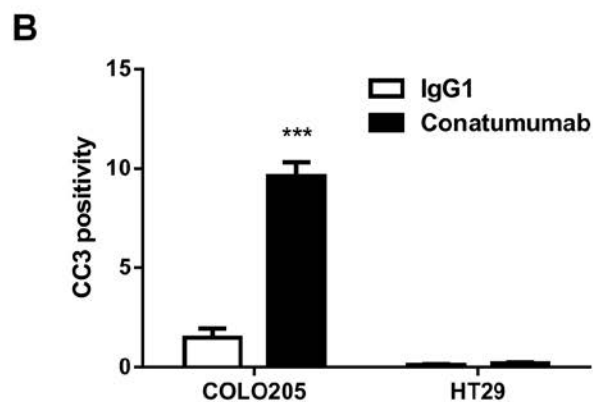
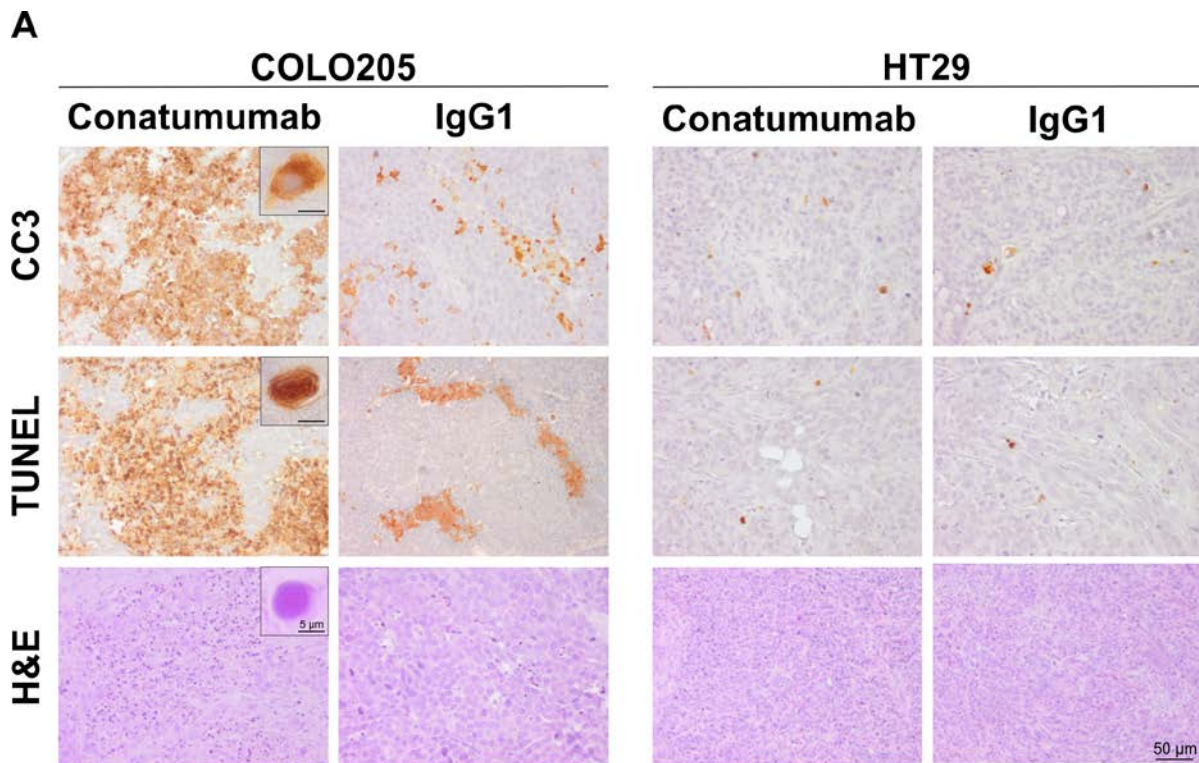
Supplemental Figure 3. Tumor volumes recorded by caliper measurements of COLO205 (A) and HT29 (B) tumor-bearing mice at baseline and after IgG1 or conatumumab treatment.



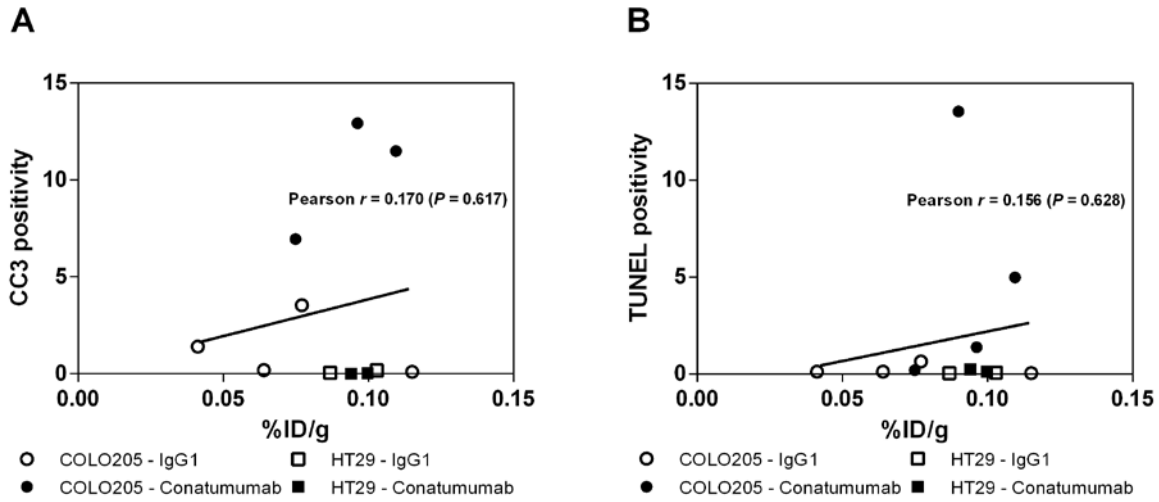
Supplemental Figure 4. Representative pseudo-color autoradiography (ARG) images of COLO205 (A) and HT29 (B) whole tumor slices from mice injected with ^{99m}Tc -linear duramycin after IgG1 or conatumumab treatment.



Supplemental Figure 5. *Ex vivo* ^{99m}Tc -duramycin, ^{18}F -FDG and ^{99m}Tc -linear duramycin organ biodistribution (%ID/g) of COLO205 (A) and HT29 xenografts (B) 24 hours after IgG1 or conatumumab treatment.



Supplemental Figure 6. Representative microscopic images of adjacent COLO205 and HT29 tumor slices stained with CC3, TUNEL and H&E acquired at x20 and x63 (inset) magnification. Cells in brown were positive for cleaved caspase-3 (CC3) and TUNEL staining (A). Densitometric analysis of CC3 (B) and TUNEL (C) staining. *******, $P < 0.001$, significantly different from IgG1.



Supplemental Figure 7. Correlation analysis of radiotracer uptake to histological measurement of tumor cell death. CC3 (A) and TUNEL staining (A) were compared with tumor-associated ^{99m}Tc -linear duramycin radioactivity measured *ex vivo* in the tumors (%ID/g).

SUPPLEMENTAL TABLES

Supplemental Table 1. Blood glucose levels in COLO205 and HT29 xenografts at baseline and after therapy

Scan	COLO205		HT29	
	IgG1	Conatumumab	IgG1	Conatumumab
Baseline (mg/dL)	68.6 ± 9.4	82.5 ± 2.3	58.2 ± 9.1	62.5 ± 7.4
Post treatment (mg/dL)	87 ± 6.5	77.4 ± 7.3	67.8 ± 13.5	52.8 ± 3.3

Data are mean ± SEM

Supplemental Table 2. Uptake of ¹⁸F-FDG in COLO205 and HT29 xenografts at 24 hours post treatment and tumor-to-background ratios

Parameter	COLO205		HT29	
	IgG1	Conatumumab	IgG1	Conatumumab
Blood uptake (%ID/g)	0.49 ± 0.06	0.48 ± 0.07	0.47 ± 0.01	0.48 ± 0.03
Muscle uptake (%ID/g)	0.22 ± 0.03	0.21 ± 0.03	0.23 ± 0.01	0.20 ± 0.02
T/B ratio	4.95 ± 0.81	6.02 ± 1.09	3.74 ± 0.21	4.09 ± 0.55
T/M ratio	11.60 ± 1.47	13.71 ± 2.65	7.74 ± 0.34	8.47 ± 1.01

Data are mean ± SEM

Supplemental Table 3. Uptake of ^{99m}Tc-linear duramycin in COLO205 and HT29 xenografts and tumor-to-background ratios

Parameter	COLO205		HT29	
	IgG1	Conatumumab	IgG1	Conatumumab
Blood uptake (%ID/g)	0.028 ± 0.004	0.026 ± 0.001	0.038 ± 0.001	0.035 ± 0.002
Muscle uptake (%ID/g)	0.014 ± 0.002	0.013 ± 0.001	0.021 ± 0.001	0.025 ± 0.002
T/B ratio	2.91 ± 0.57	3.57 ± 0.41	2.46 ± .18	2.74 ± 0.24
T/M ratio	5.31 ± 0.70	7.02 ± 0.43	4.62 ± 0.73	3.83 ± 0.14

Data are mean ± SEM

References

1. Elvas F, Vangestel C, Pak K, et al. Early Prediction of Tumor Response to Treatment: Preclinical Validation of ^{99m}Tc -Duramycin. *J Nucl Med*. 2016;57:805-811.
2. Deleye S, Heylen M, Deiteren A, et al. Continuous flushing of the bladder in rodents reduces artifacts and improves quantification in molecular imaging. *Mol Imaging*. 2014;13.
3. Varghese F, Bukhari AB, Malhotra R, De A. IHC Profiler: an open source plugin for the quantitative evaluation and automated scoring of immunohistochemistry images of human tissue samples. *PLoS One*. 2014;9:e96801.